*Particle Accelerators*
1984 Vol. 15 pp. 115–136
0031-2460/84/1502–0115$18.50/0



# DETUNING EFFECT IN A TRAVELLING-WAVE ELECTRON LINAC

S. ARAI, K. KOBAYASHI, E. TOJO and K. YOSHIDA

*Institute for Nuclear Study, University of Tokyo*
*Tanashi-shi,*
*Tokyo 188, Japan*

(*Received March 23, 1983*)

Detailed measurements of acceleration characteristics have been performed on a 15-MeV S-band travelling-wave electron linac. A remarkable feature of the results is that the energy gain, as well as the energy spread, of the output beam are optimized when the linac is operated with a microwave frequency higher than the tuned frequency of the accelerator waveguide. The difference between this optimum frequency and the tuned frequency grows as the beam intensity is increased and amounts to 250 kHz when the beam intensity is as high as 350 mA.

The results of analysis show that the linac is detuned by reactive beam loading and that the detuning effect is partly compensated by changing the operating microwave frequency to be higher than the tuned frequency.

## 1. INTRODUCTION

A 15-MeV S-band travelling-wave electron linac is operated as the injector for the 1.3-GeV electron synchrotron at the INS (Institute for Nuclear Study, University of Tokyo). The INS linac[1] consists of a single accelerator waveguide with a buncher section in it, as usual for similar-scale linacs.

It has been found out in operation that the capture efficiency of injection beam by the synchrotron is improved when the linac is operated with a microwave frequency higher than the tuned frequency of the accelerator waveguide. It has also been found that the difference between the optimum frequency and the tuned frequency grows as the beam intensity of the linac is increased.

This indicates that beam loading influences the accelerating field in the linac and deteriorates the accelerated-beam quality and that the effect of beam loading can be compensated to some extent by increasing the operating frequency. The acceleration efficiency can also be improved by temperature adjustment of the buncher section.[2] In this case, the tuned frequency of accelerator waveguide is changed instead of the operating frequency.

For a travelling-wave electron linac, a beam-loading effect resulting in a resonant-frequency shift of the accelerator waveguide has been so far unexpected, although it has been extensively studied for standing-wave cavities.[3–10]

The resonant frequency of a standing-wave cavity is known to change when it is loaded with charged particles to be accelerated by the electric field in it. The phenomenon observed in the INS electron linac suggests that the resonant-frequency shift due to beam loading is also significant in a travelling-wave accelerator structure. This effect, which deteriorates the beam quality, is especially serious for the injector linac of an electron synchrotron because it is required to provide a beam with as small energy spread as possible.

In advance of the present work, a basic theory for the detuning effect in travelling-wave accelerator structures has been developed analytically and has been proved experimentally by using a test waveguide with constant impedance, as mentioned in the immediately preceding paper "Detuning Effect in a Travelling-Wave Accelerator Structure due to Beam Loading".[11]

Based on the above study, the detuning effect due to beam loading on the INS linac has been studied experimentally and theoretically. The emphasis is on measurements on the acceleration characteristics such as the capture efficiency for injection beam and the momentum and momentum spread of output beam. In addition, the phase shifts of the accelerating field are examined relative to the operating frequency and the accelerated beam intensity. Since beam-loading effects in steady-state acceleration are of interest in the present study, the accelerated beam and the accelerating field are observed in the period after the microwave filling time of the accelerator waveguide. These experimental results are interpreted by applying a theory which has been developed in the above paper[11] to the beam-trace calculations.

## 2. EXPERIMENT

### *2.1. Outline of the Linac*

The linac used in the present study can accelerate an electron beam of 250 mA to 15 MeV in a 2-m long waveguide with 7 MW of microwave power. The buncher and regular section are united in a body to form a single accelerator waveguide. A periodic disk-loaded structure of 2/3-$\pi$ mode is used and the tuned frequency is 2758.00 MHz at 30°C.

The specifications of the linac are summarized in Table I. As shown in Fig. 1, the buncher section consists of three constant-impedance segments. The length of each segment is equal to one guide wavelength. The phase velocity and the group velocity of the microwave change stepwise, as shown in Table II. The regular section consists of four constant-impedance segments and the electric-field strength in the waveguide varies stepwise, but is constant on the average along the accelerator waveguide. The length of each segment is equal to four times the guide wavelength, except for the second segment, whose length is equal to five times the guide wavelength.

TABLE I

Specifications of INS Linac

| | |
|---|---|
| Length of accelerator waveguide | ~215 cm |
| Number of cavities in buncher section | 9 in 3 segments |
| Number of cavities in regular section | 51 in 4 segments |
| Phase shift per cavity | $\frac{2}{3}\pi$ |
| Tuned frequency | 2758.00 MHz (at 30°C) |
| Unloaded $Q$ | 11700 |
| Total voltage attenuation | 0.45 neper |
| Filling time | 0.5 μ sec |
| Microwave power | 7 MW |
| Gun voltage | 100 kV |
| Energy gain (loaded) | 15 MeV |
| Beam current | 250 mA |
| Energy spread | ~5% |
| Beam pulse length | 2 μ sec |
| Repetition rate | 21.5 pps |

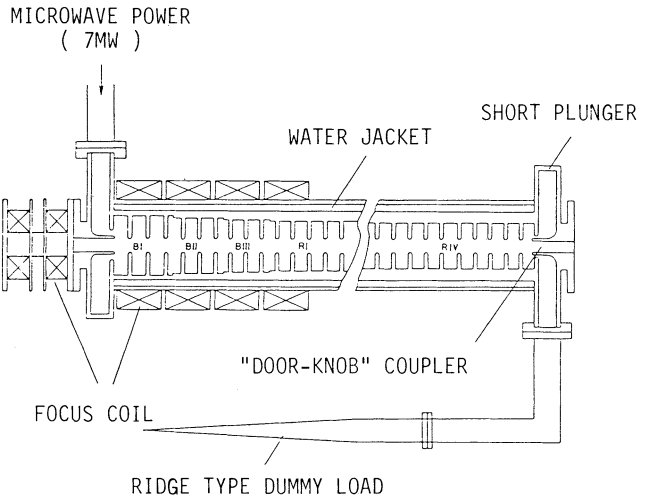


FIGURE 1 Cross-sectional view of the INS electron linac. BI ~ BIII and RI ~ RIV represent buncher and regular section, respectively.

In the design of this accelerator waveguide, resistive beam loading is taken into account but the effect of reactive beam loading is not. The disks and the cylinders have been manufactured with a tolerance of $\pm 5$ μm, to keep the tuning error of the waveguide below $\pm 100$ kHz. The measured microwave characteristics of each segment are summarized in Table II. The tuning accuracy of the segment is confirmed by measurements to be as designed.

The microwave coupler is of the "door-knob" type, which can produce an axially symmetric field at the coupler. The voltage standing-wave ratios of the couplers are flat over the frequency range of interest.

The electrons are subject to transverse forces in the buncher section since their velocities are slower than the velocity of light and they are not on the crest of the electric field. Four solenoidal coils are therefore located at the buncher section and the entrance of the regular section as seen in Fig. 1. The length of each coil is 10 cm.

TABLE II

Microwave Characteristics of the Accelerator Waveguide

| | $f_0$ (MHz) | $v_p/c$ | $v_g/c$ | $r_0$ (MΩ/m) |
|---|---|---|---|---|
| BI[a] | 2758.069 | 0.7753 | $3.09 \times 10^{-2}$ | 29 |
| BII | 2758.027 | 0.9746 | 2.39 | 49 |
| BIII | 2758.059 | 0.9908 | 2.26 | 50 |
| RI[a] | | 1.0000 | 1.86 | 50 |
| RII | | 1.0000 | 1.62 | 53 |
| RIII | 2758.005 | 1.0000 | 1.13 | 55 |
| RIV | 2758.027 | 1.0000 | 0.79 | 58 |

[a] B and R in the first column mean the buncher and the regular sections respectively. $f_0$, $v_g/c$ and $r_0$ are experimental values.

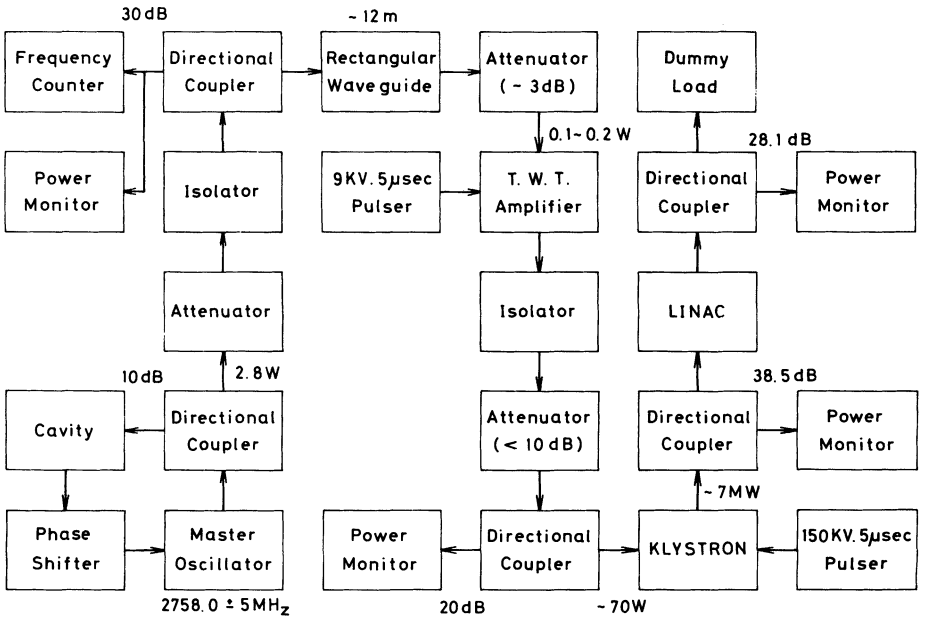


FIGURE 2 Block diagram of the microwave system of the INS linac.

A block diagram of the microwave system of the linac is shown in Fig. 2. The master oscillator is composed of a transistor microwave amplifier and a feedback loop including a high $Q$ cavity. The oscillation frequency can be adjusted by changing the resonant frequency of the cavity in the feedback loop. The cooling water of the accelerator waveguide is also circulated to the cavity of the master oscillator so that the master oscillator can follow changes of the tuned frequency of the linac due to temperature variation of the cooling water. The temperature accuracy of the cooling water is 30°C $\pm$ 0.5°C.

The output power of the master oscillator is amplified by a travelling-wave tube to a power of 1 kW with a pulse width of 5 μsec. The microwave pulse is finally amplified by a klystron to about 7 MW. The input power to the accelerator, the reflected power from the accelerator and the penetrating power are monitored by directional couplers.

The accelerating voltage of the gun is 100 kV. The emission current is adjusted by changing the bombarder voltage between the filament and the cathode. The beam from the electron gun is collimated to have a diameter of 8 mm and is controlled so that it is accelerated along the axis of the waveguide by means of horizontal and vertical steering magnets.

### *2.2. Measurement Method*

The experimental setup is illustrated in Fig. 3. The amounts of input and output beam current are measured by ferrite-core monitors current transformers installed at the entrance and the exit of the linac. These monitors have been calibrated with a Faraday cup.

The momentum and momentum spectrum of the accelerated beam are measured by a magnetic spectrometer system, as shown in Fig. 4. The system is composed of a

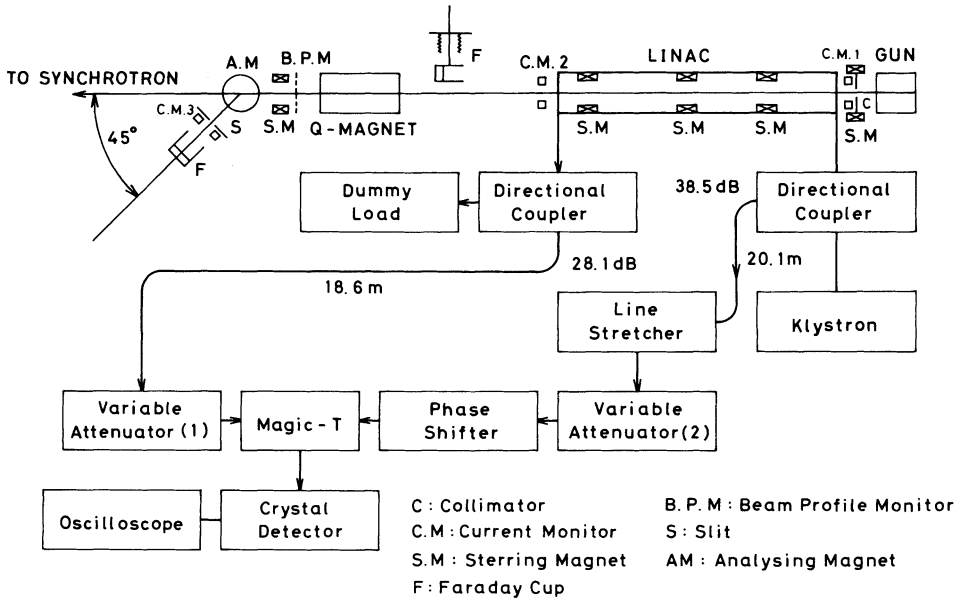


FIGURE 3 Schematic diagram of the experimental setup.

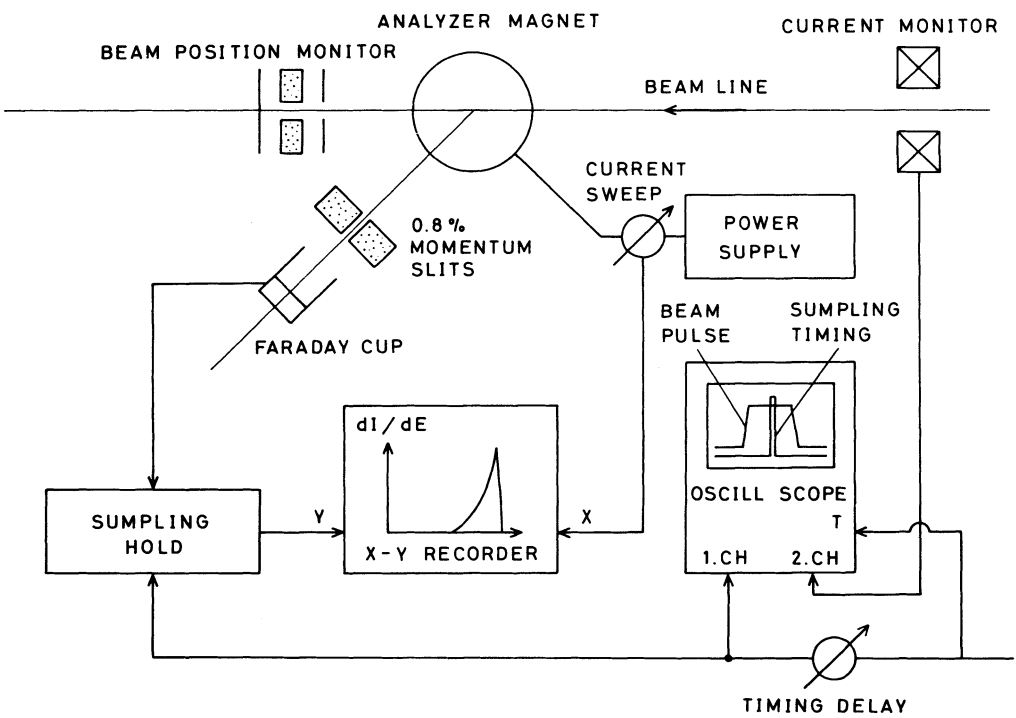


FIGURE 4 Block diagram of the momentum analyzer system.

magnet with a bending angle of 45°, a slit of 2 mm aperture set at the exit of the magnet, a Faraday cup behind the slit and an incident beam-position monitor. The momentum resolution of the system is $\pm 0.4\%$.

In order to observe the momentum spectrum of the beam accelerated in the steady state, the beam current within a 0.5-μsec duration after the transient time is detected by use of a sample-and-hold circuit. The output of the sample-and-hold circuit and the excitation current of the spectrometer magnet are displayed on a X-Y recorder. An example of the momentum spectrum thus obtained is shown in Fig. 5.

Phase variations of the accelerating field due to beam loading are measured by comparing the phases of the input and the output microwaves of the linac. These microwave signals are picked up from two directional couplers at the entrance and the exit of the accelerator waveguide, as shown in Fig. 3. The microwave signal from the upstream end of the linac is transmitted to a magic-$T$ through a variable phase shifter, while the signal from the downstream end is transmitted to the magic-$T$ through a variable attenuator. The vector sum of these microwaves is detected by a crystal detector and displayed on an oscilloscope. The phase shifter is always adjusted so that the vector sum is minimized. The difference of the readings of the phase shifter when the beam is and is not accelerated gives the phase shift of the accelerating field due to beam loading. In the measurement, the amplitudes of the two signals to the magic-$T$ are adjusted by the variable attenuator to be approximately equal for measurement accuracy. The phase shift caused by the attenuator is corrected in the data reduction.

The above-mentioned measurements have been performed by changing the beam current and the operating microwave frequency.

## 3. DATA REDUCTION AND EXPERIMENTAL RESULTS

The capture efficiency, the momentum and the momentum spread of the output beam, which determine the fundamental acceleration characteristics of the linac, are obtained from the measured results on input and output beam current and on momentum spectrum as discussed below.

The frequency dependence of the capture efficiency is expressed as the variation of output beam current at a constant input current as shown in Fig. 6.

As seen in the example of the momentum spectra shown in Fig. 5, the spectrum shows a single peak at lower frequencies, whereas it has two peaks at high frequencies. The momenta corresponding to these peaks have been recorded as the momenta of the output beams. When the beam current is increased, the frequency being constant, the momentum decreases linearly as shown in Fig. 7. For an operating frequency of 2758.5 MHz, the spectrum shows two peaks and therefore a pair of lines is obtained.

The momentum spread of the output beam is defined in two ways. One is the full width at half maximum of the spectrum and the other is given by the momentum spread for which 90% of the beam current is included.

The data obtained are processed statistically and their accuracy is evaluated.[12] The errors in the measurement may be composed of reading errors and of errors in settings such parameters as operating frequency, beam current, beam steering-coil current, microwave power level, waveguide temperature and so on. In the statistical treatment of the data, these errors have been assumed to have Gaussian distributions.

The frequency dependence of the momentum is shown in Fig. 8. The frequency dependences of the momentum apread defined by FWHM and by 90% beam current are shown in Fig. 9 and in Fig. 10, respectively.

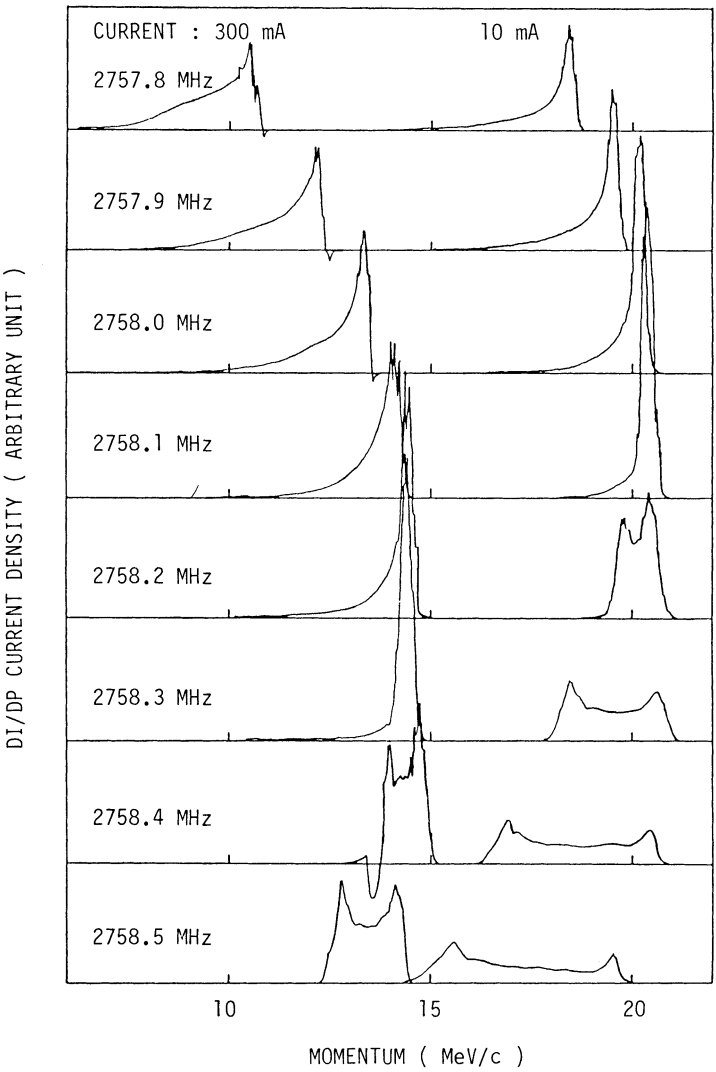


FIGURE 5 Momentum spectra for various operating frequencies and output beam currents.

The solid lines and the error bars marked on the data points indicate the most probable values and the estimated maximum errors, respectively.

An important result of the experiment is that when the operating frequency is swept from lower to higher values there are frequencies for which the output beam current or the momentum gain is maximized or the momentum spread is minimized.

The beam-loading dependence of the operating frequency to maximize output beam current is shown in Fig. 11. The beam-loading dependences of the optimum frequency for momentum and the momentum spread are shown in Figs. 12 and 13, respectively.

The experimental results can be summarized as follows: As the degree of beam loading is increased, the optimum frequencies for capture efficiency, momentum and

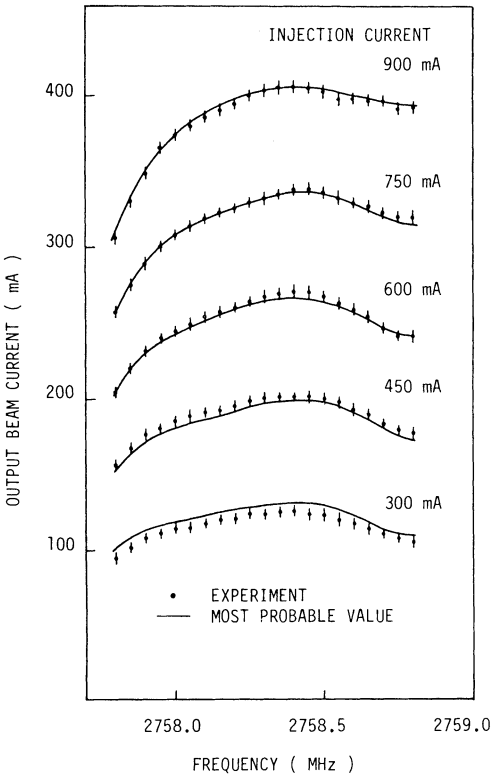


FIGURE 6 Frequency dependence of the output beam current for various injection currents.

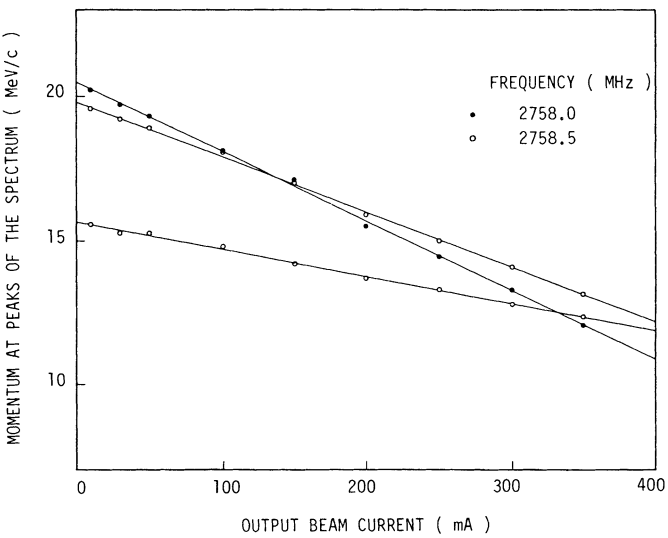


FIGURE 7 Change of beam momentum with output beam current at frequencies 2758.0 MHz and 2758.5 MHz.

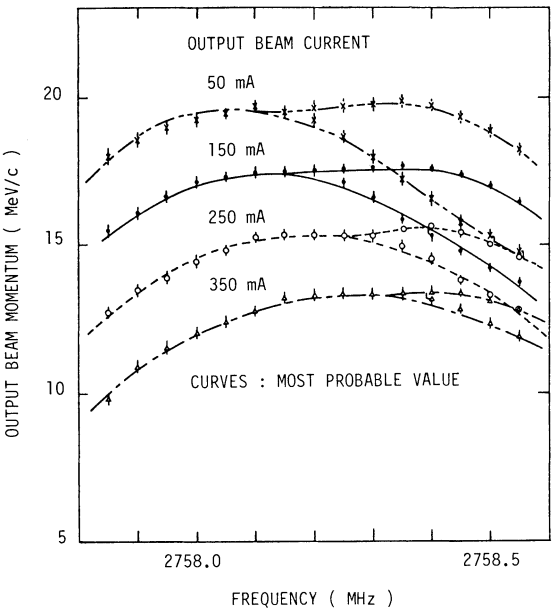


FIGURE 8 Frequency dependence of the output beam momentum with different output beam current

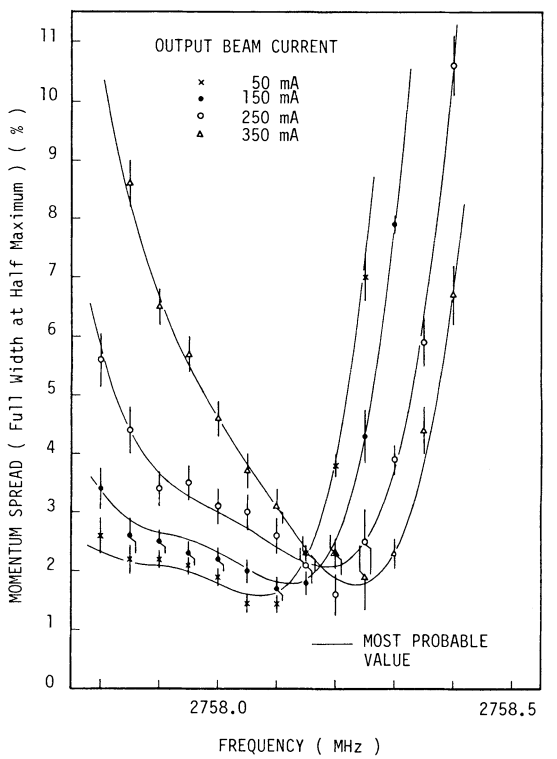


FIGURE 9 Frequency dependence of momentum spread defined as full width at half maximum.

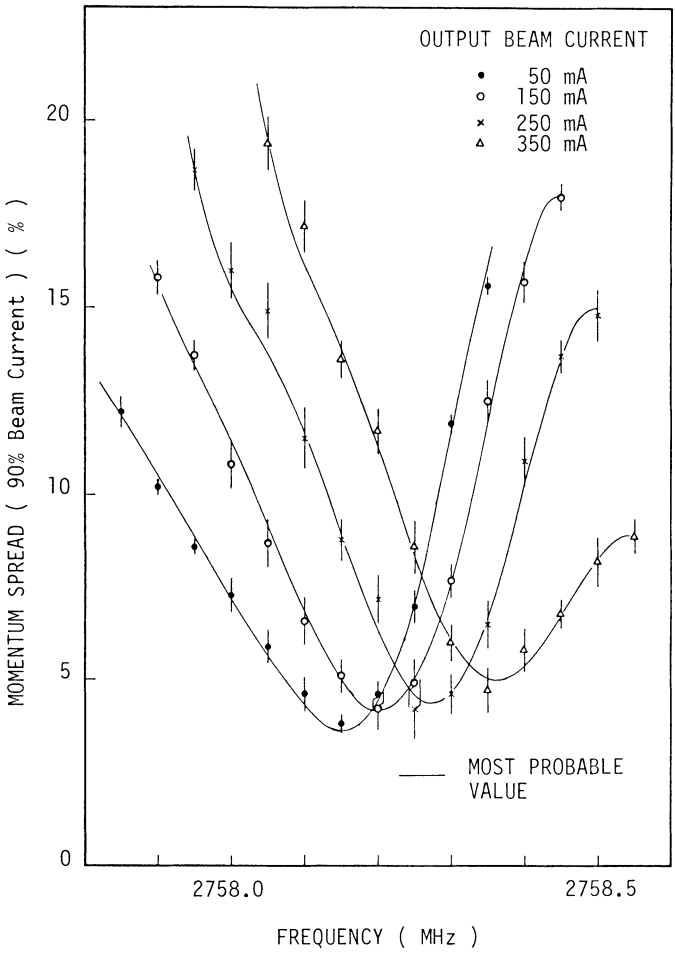


FIGURE 10 Frequency dependence of momentum spread defined by 90% beam current.

momentum spread change to frequencies higher than the tuned frequency of the accelerator waveguide. The variation of the optimum frequencies can be expressed as a linear function of the output beam current. The gradients of the optimum frequency with respect to beam current are $0.65 \pm 0.01$ MHz/A for momentum gain, and $0.60 \pm 0.02$ MHz/A and $0.67 \pm 0.03$ MHz/A for momentum spread defined by FWHM and 90% current, respectively. The gradient for the capture efficiency is rather small. The optimum frequencies at no beam loading are 2758.03 MHz for momentum and 2758.04 MHz for momentum spread (FWHM), which agree with the tuned frequency of the accelerator waveguide to within the error. As for the capture efficiency, the optimum frequency at no beam loading is close to 2758.4 MHz.

The experimental results on the phase shift of accelerating field are shown in Fig. 14. When the linac is operated at the tuned frequency, the phase of the accelerating field shifts forward, largely due to beam loading. By operating with a frequency higher than the tuned one, the phase shift is suppressed.

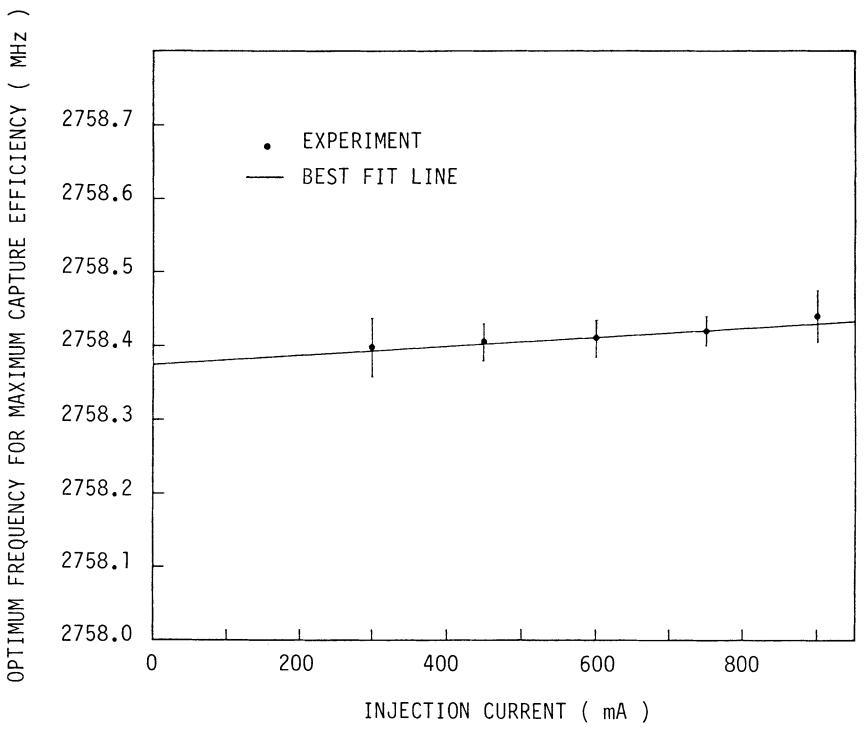


FIGURE 11 Relation between the frequency for maximum capture efficiency and injection beam current.

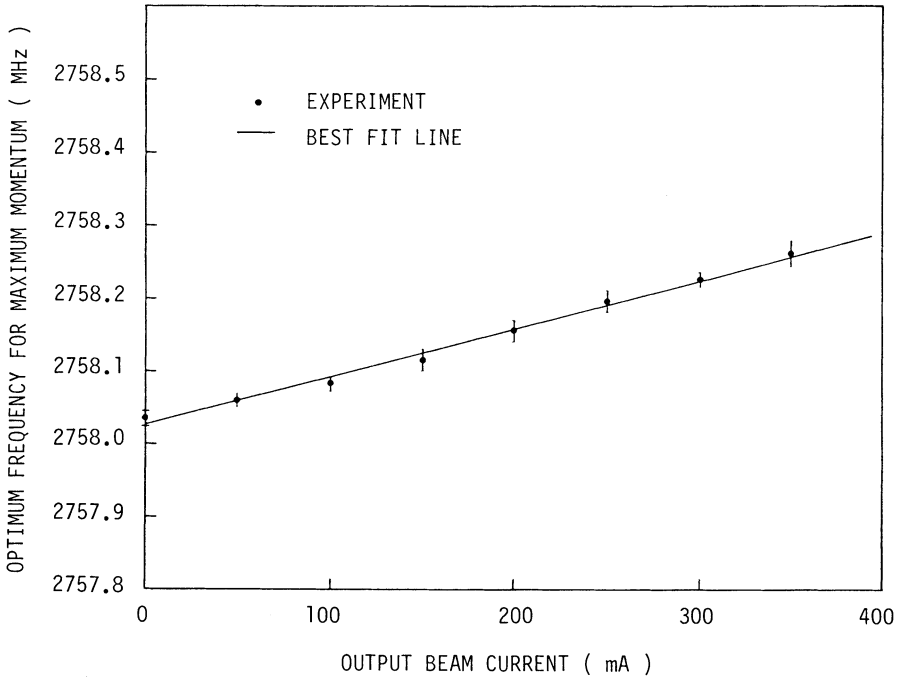


FIGURE 12 Relation between the frequency for maximum momentum and output beam current.

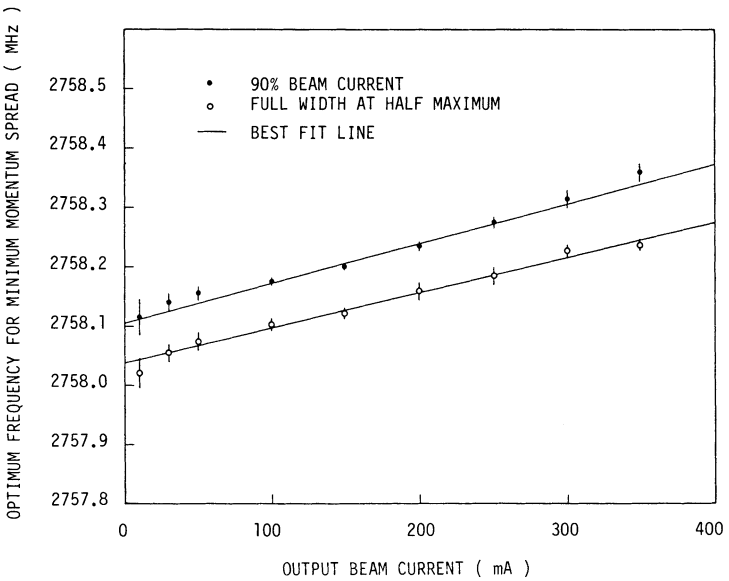


FIGURE 13 Relation between the frequency for obtaining minimum momentum spread and output beam current.

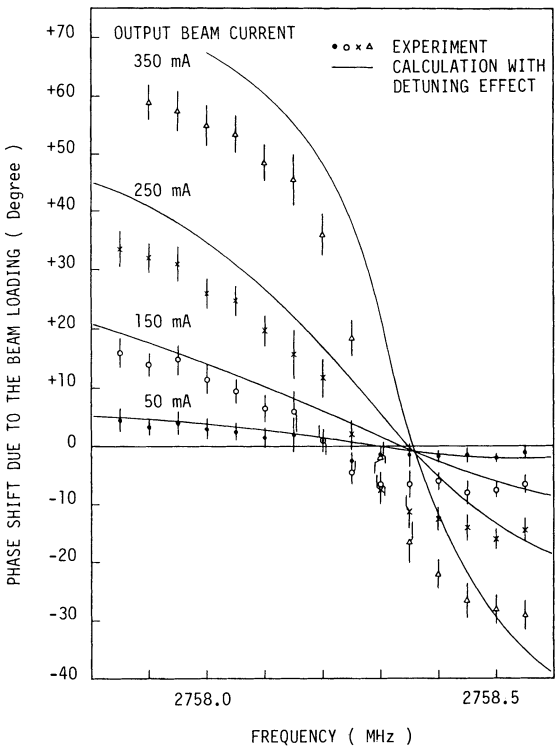


FIGURE 14 Phase shift of accelerating field due to beam loading.

## 4. THEORETICAL ANALYSIS

### *4.1. Beam-Trace Calculation*

In order to explain theoretically the experiment results presented in the preceding section, a beam-trace calculation is performed based on the theory developed in the companion paper.[11] In that paper, it is shown that reactive beam loading detunes the accelerator waveguide and causes phase variation as well as amplitude variation in the accelerating field. In the present analysis, therefore, the phase variation is derived from the tuned-frequency shift of the waveguide, which is calculated to compare with the shift of optimum operating frequency.

In the calculation, the following assumptions are made: 1) Even if the operating frequency is changed from the tuned frequency of the accelerator waveguide, or the tuned frequency varies due to beam loading, the group velocity of the microwave does not change. 2) Microwave reflection from the input coupler and the accelerator structure due to detuning is neglected. 3) The value of the phase shift due to beam loading when the linac is operated with a frequency different from the original tuned frequency is obtained by the same procedure as for the operation with the tuned frequency. 4) The cross section of the beam is a circle in which charge density is uniform.

The calculation is carried out with representative electrons that initially are at 72 microwave phases with intervals of 5°.

First the longitudinal motion of the electrons is treated. An electron of charge $e$ gains an energy of $-eE \sin \Delta$ Joules per unit length when it rides at the phase $\Delta$ of an accelerating field with an amplitude $E$. Measuring the longitudinal distance $z$ in units of free-space wavelength $\lambda_0$, the equation of motion[13] is expressed in terms of $\xi = z/\lambda_0$ as

$$\frac{\delta\gamma}{\delta\xi} = -\alpha \sin \Delta, \tag{5-1}$$

where $\gamma$ is the total energy of the electron in units of rest energy, $m/m_0$,

$$\gamma = \frac{m}{m_0} = \frac{1}{\sqrt{1 - \beta_e{}^2}},$$

$\beta_e$ being the velocity divided by the velocity of light $c$ and $\alpha$ is the normalized electric field intensity,

$$\alpha = \frac{eE\lambda_0}{m_0 c^2}.$$

The electron phase is obtained by considerating both the electron and the phase velocities. Representing the wave phase velocity divided by the velocity of light by $\beta_p$, the phase $\Delta$ at the position $\xi + \delta\xi$ is

$$\Delta(\xi + \delta\xi) = \Delta(\xi) + 2\pi \cdot \delta\xi \left(\frac{1}{\beta_p} - \frac{1}{\beta_e}\right). \tag{5-2}$$

Equation (5-2) is accurate only when the phase of the accelerating field is not affected by beam loading. To take the phase shift $\Delta\psi$ due to beam loading into account, Eq. (5-2) is corrected to

$$\Delta(\xi + \delta\xi) = \Delta(\xi) + 2\pi \cdot \delta\xi \left(\frac{1}{\beta_p} - \frac{1}{\beta_e}\right) - \Delta\psi. \tag{5-3}$$

In order to evaluate the phase shift $\Delta\psi$, the detuning of the accelerator waveguide and the variation of the accelerating field are discussed below. When the bunch rides at the phase $\phi_b$ of the accelerating field $E_0$ at position $\xi$, with the velocities of the bunch and the microwave being taken to be approximately equal to each other between $\xi$ and $\xi + \delta\xi$, the electric field at position $\xi + \delta\xi$ is expressed in the following form,[11]

$$E(\xi + \delta\xi) = \{E_0(\xi)e^{-(\omega\lambda_0\delta\xi/2v_gQ_0)} - FI_0re^{j\phi_b}(1 - e^{-(\omega\lambda_0\delta\xi/2v_gQ_0)})\}e^{j(\omega t - k\lambda_0\xi)}, \tag{5-4}$$

where $v_g$ is the group velocity of the wave, $Q_0$ is the unloaded $Q$, $F$ is the form factor of the bunch, $I_0$ is the mean beam current during one pulse and $r$ is the peak shunt impedance per unit length. $E_0$ is the superposition of the driving field and the beam-induced field. The first term of Eq. (5-4) shows the attenuation of the accelerating field and the second term represents the amplitude of the electric field induced by beam passing from $\xi$ to $\xi + \delta\xi$.

The electron beam is initially uniform over the wave phase and goes gradually into bunches in its passage from the buncher to the upstream end of the regular section. Therefore the bunch form factor $F$ which affects the magnitude of the beam-induced field, and the effective loading angle $\phi_b$, which is defined as the weighted mean value of the bunch phase, can be found along the accelerator waveguide (See Appendix A).

Replacing $FI_0r$ with $E_b$ and attenuation factor $\exp(-(\omega\lambda_0\delta\xi/2v_gQ_0))$ with $T$, the electric field amplitude at the position $\xi + \delta\xi$ is given as

$$E_0(\xi + \delta\xi) = [\{E_0(\xi)T - E_b(1 - T)\cos\phi_b\}^2 + E_b^2(1 - T)^2\sin^2\phi_b]^{1/2}. \tag{5-5}$$

The tuned-frequency shift of the accelerator waveguide can be, in principle, caused by both resistive and reactive beam loadings. However, the effect of resistive loading on the tuned-frequency shift can be ignored[8,11] and only the effect of reactive loading is taken into account here. The tuned-frequency shift of the waveguide at position, $\xi + \delta\xi$, is given by[11]

$$\Delta f = -\frac{f_0'}{2Q_0} \frac{E_0(\xi)TE_b\sin\phi_b}{E_0^2(\xi)T^2 + E_b^2(1 - T)^2 - 2E_0(\xi)TE_b(1 - T)\cos\phi_b}, \tag{5-6}$$

where $f_0$ is the tuned frequency with no beam loading.

The phase shift of the accelerating field due to beam loading is obtained by using the equation above as

$$\Delta\psi = 2\pi f\lambda_0\,\delta\xi \left\{\frac{1}{v_p} - \frac{v_g + (f - f_0 - \Delta f)\lambda_g}{fv_g\lambda_g}\right\}, \tag{5-7}$$

where $v_p$ represents the phase velocity of the wave in the accelerator waveguide when the operating frequency is $f$, and $\lambda_g$ is the guide wavelength.

By substituting the phase shift given by Eq. (5-7) into Eq. (5-3), and using Eq. (5-1), the longitudinal motion of electrons can be described completely. The total energy $\gamma$ of an electron at position $\xi + \delta\xi$ is given by

$$\gamma(\xi + \delta\xi) = \gamma(\xi) - \alpha(\xi) \sin \Delta(\xi)\, \delta\xi. \tag{5-8}$$

The initial value $\gamma(0)$ is decided by the voltage of the electron gun, which is 100 kV for the INS linac. The electric-field intensity $\alpha(\xi)$ is given by

$$E(\xi) = \sqrt{\frac{\omega r P(\xi)}{v_g Q_0}} \tag{5-9}$$

Last, the problem on the beam-intensity decrease in the course of acceleration is described below. Beam loss in the accelerator waveguide is important since the beam intensity determines the microwave power loss and the degree of detuning of the accelerator waveguide. The beam loss is caused by collisions with the disks or by the deceleration by the microwave field. The diameter of the beam just injected to the linac is 8 mm, determined by the collimator. It is assumed that the electrons are distributed uniformly in the beam diameter, which changes along the accelerator waveguide. The change of beam diameter is calculated by considering the transverse forces of space charge, of the microwave field and of the focusing force of the solenoid coils.[12] When the beam diameter $2a$ increases to be larger than the disk hole diameter $2a_0$, the beam intensity is regarded to decrease by a factor $a_0^2/a^2$.

### *4.2. Analytical Results*

The parameters that are necessary for the calculation, $Q_0$, $r$, $v_g$ and $P$, are known by measurement. They are in Table I and II. Since these values are accompanied by errors of nearly 10%, they are treated as variable within the errors in the calculation and are determined to reproduce the beam momentum, which is most sensitive to these parameters. With similar considerations, the angular spread of the injection beam and magnetic field of solenoid coils are decided so as to reproduce the capture efficiency, which is sensitive to these values. Using the parameters as obtained above, calculations are performed for the various operating frequencies and beam currents.

Typical results of the momentum spectrum for currents of 0 and 300 mA are given in Fig. 15. The calculated momentum spectrum and its frequency dependence agree well with the experimental result, which is shown in Fig. 5. The maximum momentum and minimum momentum spread for beam current of 300 mA are obtained at the frequency around 2758.20 MHz, while the optimum frequency for 0 mA is close to 2758.0 MHz.

The frequency dependence of output beam current, momentum and momentum spread are given in Figs. 16, 17 and 18, where calculated results are represented with solid lines in comparison with the experimental results. Theoretical results are in close agreement with experiments for all cases in the figures.

In the figures, the calculated results without taking the detuning into account are also shown with broken lines, which cannot explain the experimental results, especially the behavior at high currents. In Fig. 19, the frequencies that give the maximum

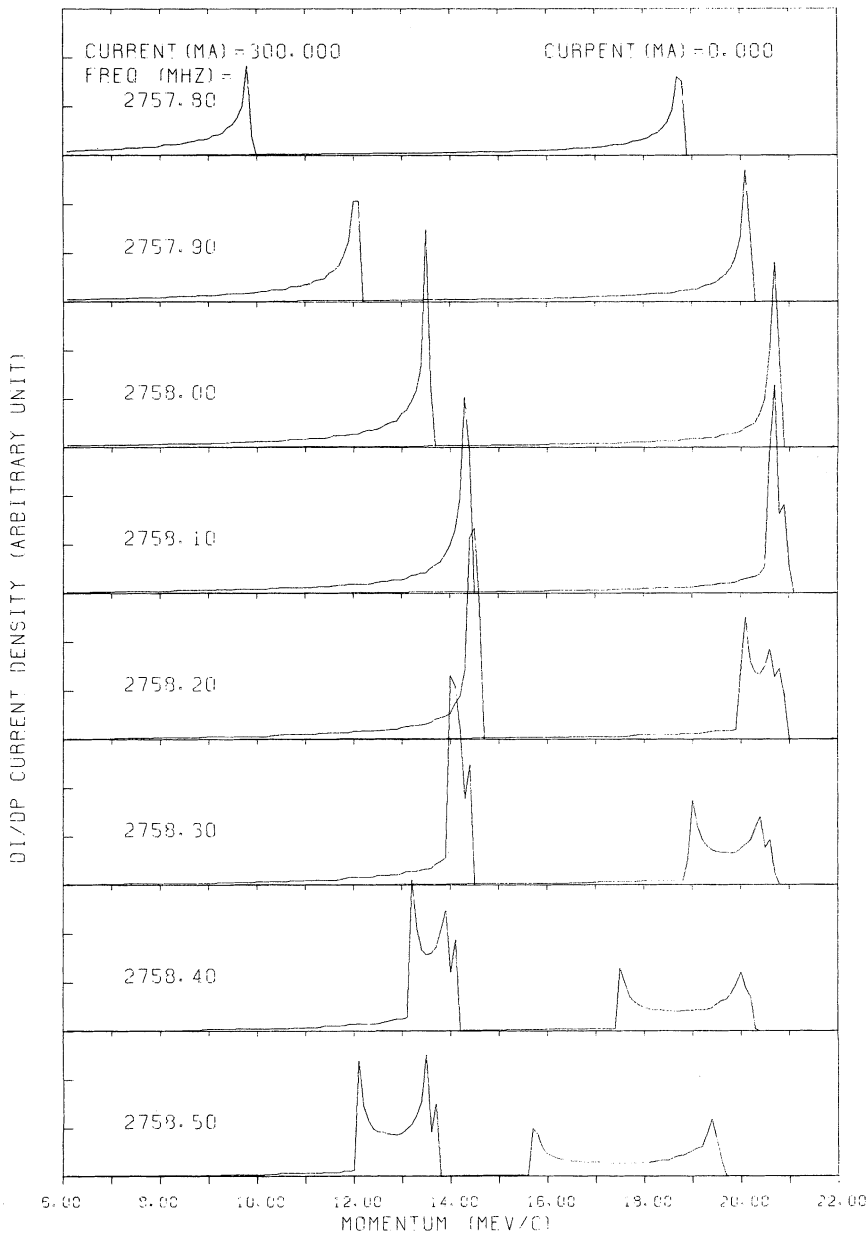


FIGURE 15 Momentum spectra for the various operating frequencies at heavy beam loading, 300 mA, and at vanishing current.

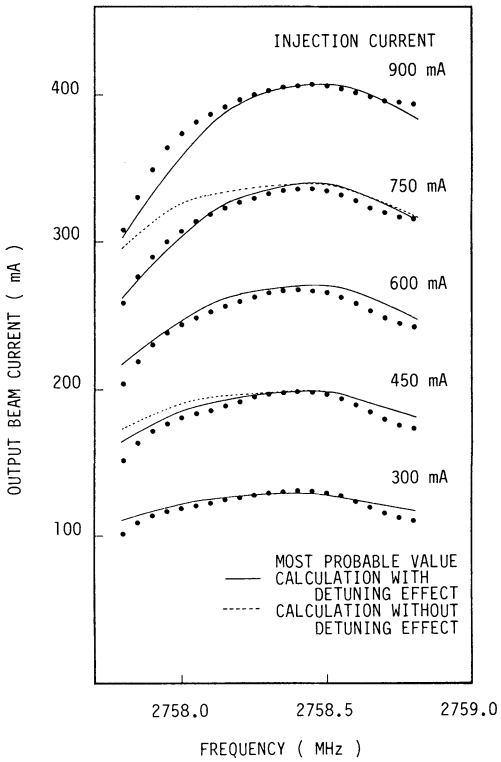


FIGURE 16 Experimental and theoretical values of output beam currents as functions of operating frequency.

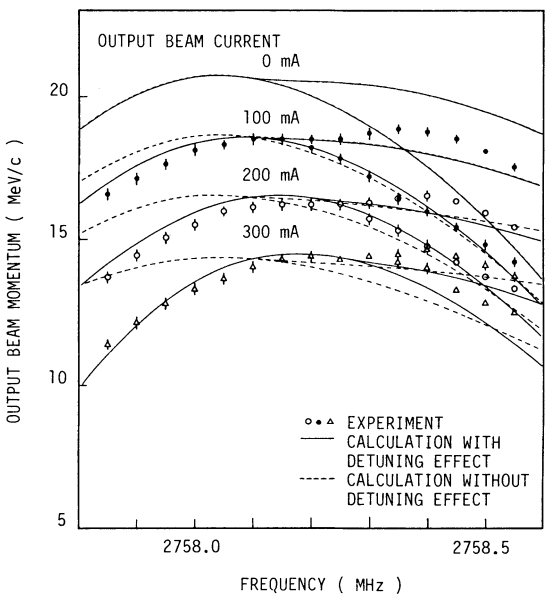


FIGURE 17 Experimental and theoretical values of the momentum at spectrum peak as functions of operating frequency.

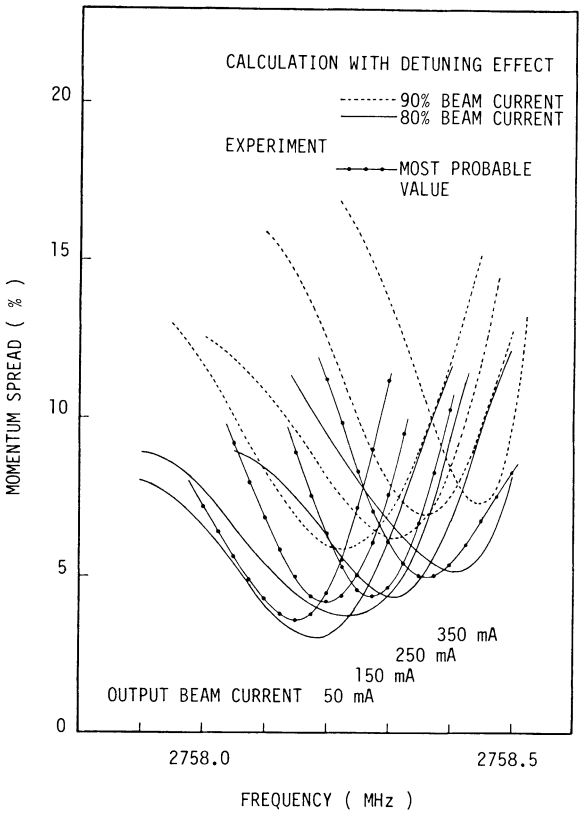


FIGURE 18 Frequency dependence of momentum spread.

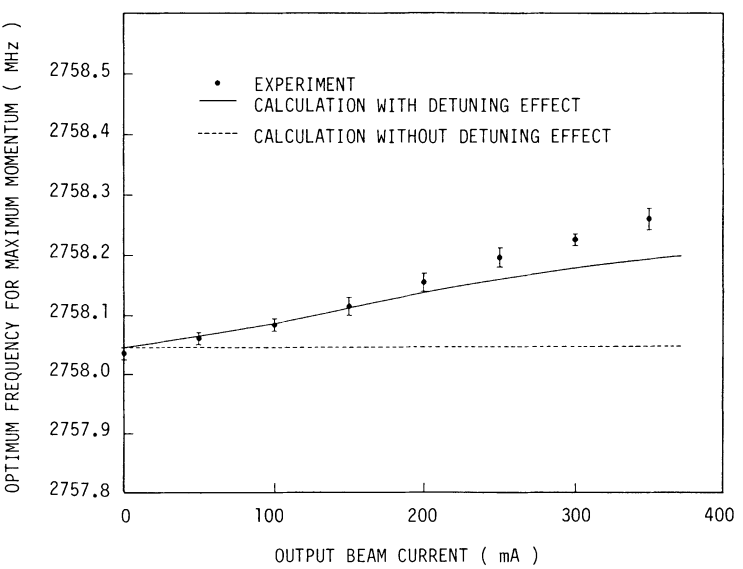


FIGURE 19 Frequency for maximum momentum as a function of output beam current.

momentum are presented as functions of output beam current. The solid line is the calculation with detuning effect and the broken line is without detuning effect. The calculated result without detuning shows that the optimum frequency is independent of the degree of beam loading, while the result with the detuning has a gradient which is consistent with the experiment.

As for the microwave phase shift, the calculated result for various frequencies and beam currents is shown in Fig. 14 together with the experimental result. The calculation explains the features of the experimental results well.

The calculation reveals the behavior of the bunch and the microwave inside the accelerator waveguide which produces the results discussed above. In Figs. 20(a) and (b), the resonant-frequency shift and the phase shift due to beam loading are shown along the accelerator waveguide. The effective loading angles of electron bunch are also plotted in the figure. Figure 20(a) shows the calculation for the operating frequency of 2758.0 MHz, which is the tuned frequency of the waveguide. As is expected, no resonant-frequency shift and therefore no phase shift occur for zero current, while they grow along the accelerator waveguide when high-current beam is accelerated. The effective loading angle moves from $-110°$ to $-170°$. Deterioration of beam quality at heavy beam loading is due to this change of loading angle. On the other hand Fig. 20(b)

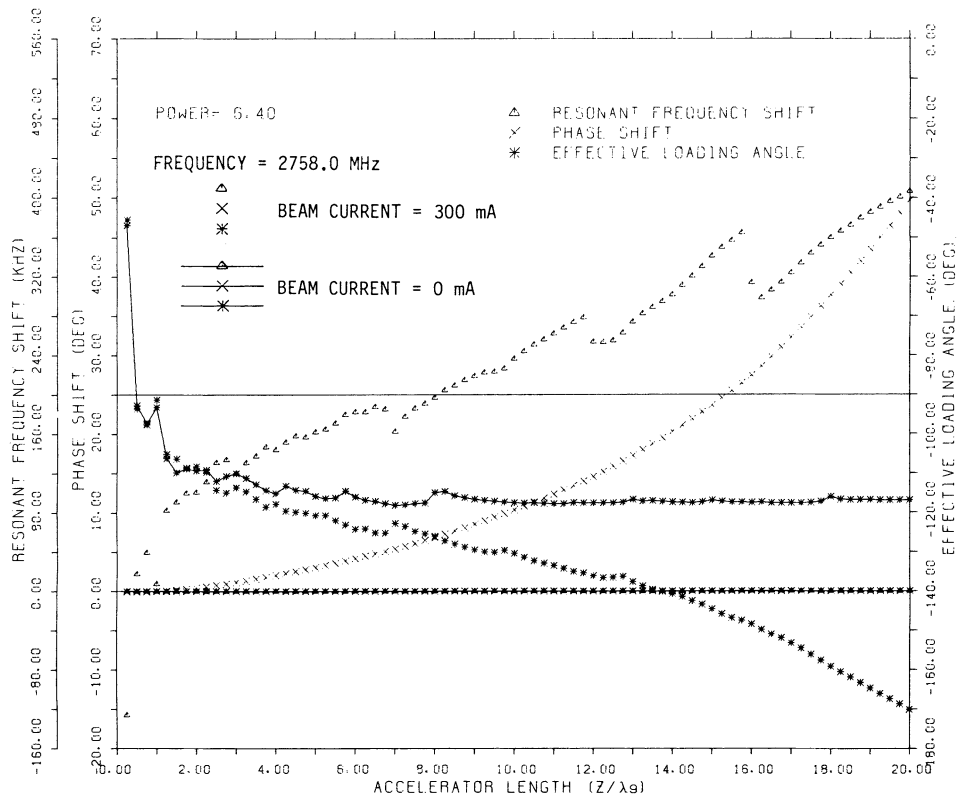


FIGURES 20(a) and (b) Calculated results of beam trace and microwave propagation along the accelerator waveguide. In Figure (a) are given the results for the operating frequency of 2758.0 MHz with the accelerated beam currents of 0 mA and 300 mA. In Figure (b) the results are presented for two operating frequencies at the beam current of 300 mA.

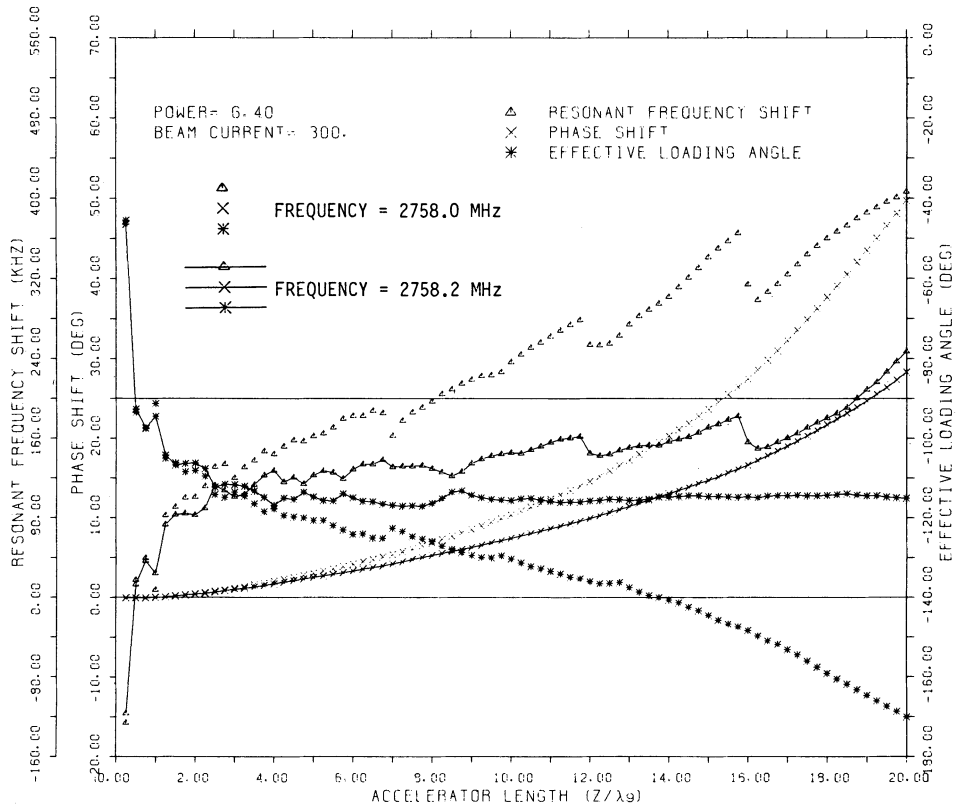


FIGURE 20(b)

shows that, if the wave frequency is changed to be 2758.2 MHz, detuning effects are well compensated and the effective loading angle is kept constant through the whole accelerator waveguide, even in high-current acceleration.

## 5. CONCLUSION

Experimental results on beam-acceleration characteristics of the INS linac can be summarized as follows; With an operating microwave frequency of 2758.0 MHz, which is the tuned frequency of the accelerator waveguide, it is impossible to achieve good beam quality when high current is accelerated. However, it is improved by increasing the operating frequency. The microwave frequency that gives maximum momentum gain or minimum momentum spread increases linearly with accelerated beam intensity. The gradients are 0.65 $\pm$ 0.01 MHz/A for the momentum gain and 0.60 $\pm$ 0.02 MHz/A for the momentum spread defined as FWHM or 0.67 $\pm$ 0.04 MHz/A for the momentum spread in which 90% of beam current is contained. These values almost agree with each other. Concerning the capture efficiency, it varies with operating frequency but does not have so much correlation with beam intensity.

The phase of the accelerating field, measured at the exit of the waveguide, shifts,

largely depending on the degree of the beam loading, but it can be compensated by operating with a frequency higher than the tuned one.

From the results of the analysis, it is concluded that the beam-acceleration characteristics of the INS linac relative to frequency can be explained by the detuning of the accelerator waveguide due to beam loading.

The slope of the optimum frequency shift with the increase of beam current is calculated to be 0.45 MHz/A, which is 70% of the experimentally obtained value. This result cannot be deduced by the calculation without taking the detuning effects into consideration.

The detuning effect is, of course, largely dependent upon the linac structure and the present numerical results are peculiar to the INS linac. The structure of the INS linac, however, is standard in electron linacs of similar size and therefore the detuning effect should be taken into account in design of future electron linacs.

## ACKNOWLEDGMENTS

The authors express their sincere gratitude to Professors K. Huke, J. Tanaka, and T. Katayama for their encouragement, suggestions and helpful discussions during the work. They are grateful to Dr. K. Ukai for his assistance in computational work, and to Dr. M. Yoshioka for his collaboration in the measurements.

We made use of the computer FACOM-180II AD at the INS computer center.

## REFERENCES

1. T. Katayama, S. Arai, K. Yoshida, and J. Tanaka, INS-Report 240 (1975).
2. Y. Torizuka, Tohoku University, private communication.
3. R. L. Gluckstern, Minutes of the Conf. on Proton Linear Accelerators, Yale University, 1963, p. 95.
4. C. S. Taylor, and Y. Dupuis, Minutes of the 1964 Conf. on Proton Linear Accelerators, MURA-714, Wisconsin, 1964, p. 239.
5. M. J. Lee, Proc. 1968 Proton Linear Accelerator Conf., BNL-50120, New York, 1968, p. 108.
6. J. S. Fraser, J. Mckeown, G. E. McMichael, and W. T. Diamond, Proc. 1967 Proton Linear Accelerator Conf., AECL-5677, Ontario, 1967, p. 166.
7. T. Nishikawa, Minutes of the 1964 Conf. on Proton Linear Accelerators, MURA-714, Wisconsin, 1964, p. 214.
8. S. Arai, T. Katayama, E. Tojyo, and K. Yoshida, *Particle Accelerators*, **11,** 103 (1980).
9. T. Katayama, T. Fukushima, and T. Yamakawa, *Jpn. J. Appl. Phys.*, **19,** 2229 (1980).
10. V. K. Neil, *Rev. Sci. Instrum.*, **33,** 169 (1962).
11. S. Arai, K. Kobayashi, E. Tojo, and K. Yoshida, *Particle Accelerators*, **15**,99 1984) (preceding paper).
12. S. Arai, INS-J-162, 1981.
13. J. M. Ponce de Leon, M. L. Report No. 265, 1955.

# APPENDIX A

## Bunch Form Factor and Effective Loading Angle

The induced field of an electron bunch which has a certain longitudinal spread can be obtained as a superposition of the induced fields by the sub-bunches defined by segmenting the bunch along the accelerating field. The segmentation should be fine enough that the bunch form factor of the sub-bunch can be regarded to be unity. In the

beam-trace calculation, a 1 electron bunch is divided in the microwave phase space into 72 bins. The microwave phase for each sub-bunch is represented as $\Delta(N)$, $N$ being 1 to 72. Each sub-bunch carries the current $I_0(N) = I_0/72$.

The electric field induced by a sub-bunch during the passage through $\delta\xi$ is

$$E_b(N) = I_0(N)r(1 - e^{-(\omega\lambda_0\delta\xi/2v_gQ_0)})e^{j\{\omega t - k\lambda_0\xi + \Delta(N)\}}. \tag{A-1}$$

and the induced field of the actual bunch is

$$E_b = r(1 - e^{-(\omega\lambda_0\delta\xi/2v_gQ_0)})e^{j(\omega t - k\lambda_0\xi)} \sum_{N=1}^{72} I_0(N)e^{j\Delta(N)}. \tag{A-2}$$

From Eqs. (A-2) and (5-4), the form factor F and the effective loading angle $\phi_b$ are

$$F = \frac{1}{I_0}\sqrt{\left\{\sum_{N=1}^{72} I_0(N)\cos\Delta(N)\right\}^2 + \left\{\sum_{N=1}^{72} I_0(N)\sin\Delta(N)\right\}^2}, \tag{A-3}$$

$$\phi_b = \tan^{-1}\left(\frac{\sum_{N=1}^{72} I_0(N)\sin\Delta(N)}{\sum_{N=1}^{72} I_0(N)\cos\Delta(N)}\right). \tag{A-4}$$